Polymer Degradation and Stability 171 (2020) 109030

Contents lists available at ScienceDirect

Polymer Degradation and Stability

journal homepage: www.elsevier.com/locate/polydegstab

The effect of introduction of filament shift on degradation behaviour of PLGA- and PLCL-based scaffolds fabricated via additive manufacturing

Ewa Walejewska [a], Joanna Idaszek [a], Marcin Heljak [a], Adrian Chlanda [a], Emilia Choinska [a], Vasif Hasirci [b], Wojciech Swieszkowski [a, *]

[a] Faculty of Materials Science and Engineering, Warsaw University of Technology, Woloska 141, 02-507, Warsaw, Poland
[b] Department of Medical Engineering, Acibadem Mehmet Ali Aydinlar University, 34752, Istanbul, Turkey

ARTICLE INFO

Article history:
Received 5 September 2019
Received in revised form
6 November 2019
Accepted 17 November 2019
Available online 24 November 2019

Keywords:
Hydrolytic degradation
Architecture modification
poly(L-lactide-co-glycolide)
poly(L-lactide-co-ε-caprolactone)
Additive manufacturing

ABSTRACT

The degradation rate of polyester scaffolds has been emphasised as one of the main areas of concern in bone tissue engineering. In ideal conditions, the degradation of polymeric constructs should match regeneration of the injured tissue. Thus, there is an imperative need to strictly define and understand determinants influencing the degradation rate of scaffolds. In this study, we focused on the effect of filament shift introduction on degradation behaviour of the polymeric-based scaffolds. The poly(L-lactide-co-glycolide) (PLGA), poly(L-lactide-co-ε-caprolactone) (PLCL) and their tricalcium-phosphate-loaded (TCP) composites containing 20 and 40 wt% of filler, were utilized to fabricate constructs using modified fused deposition modeling (FDM). The scaffolds were designed with filament lay-down pattern of 0°/90° and with or without the modifications of filament distance in n+2 layer, shifted and non-shifted constructs were obtained, respectively. To investigate the degradation profile, the change of mass, pH, water absorption and initial molecular weight (M_{w0}) loss was observed during the degradation study in phosphate buffered saline (PBS) at 37 °C for up to 48 weeks. The scaffold morphology was evaluated utilizing scanning electron microscopy (SEM) and the visualization of the topography was performed utilizing atomic force microscopy (AFM). Surface area to volume ratio (SVR) and porosity were determined using micro-computed tomography (μCT). The fluid flow simulations were used to define the permeability of two investigated groups of scaffolds. The results of this study clearly demonstrate the accelerating effect of filament shift introduction on degradation behaviour in the scaffolds with similar porosity and SVR. The decrease of M_{w0} was significantly higher in case of all shifted samples. We assume that faster degradation of shifted constructs may be attributed to their tortuosity, making them less permeable and prone to the degradation, as the result of the accumulation of acidic products in the tortuous architecture of the samples. Thus, the effect of introduction of filament shift into scaffold architecture comprise an attractive approach to influence the degradation rate in case of bone regeneration with the use of polyesters scaffolds.

1. Introduction

Development of bone tissue engineering (BTE), as an interdisciplinary field of life science, regenerative medicine and material engineering, has proposed promising strategies to heal critical bone defects at the hand of biological substitutes, so called three-dimensional (3D) scaffolds [1,2]. There are many challenges in designing and fabricating such constructs, as they should satisfy current requirements of restoration and improvement of bone growth [3]. These include i.e. biocompatibility of the material and mechanical properties, while ensuring certain porosity and osteoconductivity [4].

One of the computer-aided techniques, which gained surprisingly extensive interest and allow to meet a number of scaffold criteria, is additive manufacturing (AM) [5–7].Fused deposition modelling (FDM) is a part of AM family and has been widely adopted for fabrication of 3D objects with the use of polymeric

* Corresponding author.
E-mail address: wojciech.swieszkowski@pw.edu.pl (W. Swieszkowski).

https://doi.org/10.1016/j.polymdegradstab.2019.109030
0141-3910/

molten fibres [8–11]. Apart from obtaining controlled interconnectivity, pore size or porosity of the scaffold fabricated via FDM, a precise extruding deposition (PED), as a branch of FDM, can introduce some additional benefits to the scaffold manufacturing [12,13]. Direct extrusion of scaffolding material with the use of polymeric pellets or cut composite films is considered to be its major advantage, as it for instance, eliminates the need of filament preparation [14].

While designing and manufacturing TE scaffolds, there is a necessity to provide tissue regeneration in a particular timely manner, with simultaneous incremental degradation of implemented polymeric support [15,16]. Therefore, there is a need to focus on few scaffold parameters that can be tailored to achieve assumed degradation behaviour. To this day, a wide range of materials has been tested, showing different degradation rate, indicating polymer chemistry as one of the factor contributing degradation time [17,18]. Many studies demonstrated that degradation can be easily accelerated by using different material composition [19,20]. As an example, Park and co-workers presented that sufficient higher content of hydrophilic glycolic acid units in PLGA resulted in accelerating the degradation kinetics [21]. Idaszek and co-workers demonstrated that degradation of PCL matrix was inversely correlated to PLGA degradability in PCL/PLGA/TCP ternary composites [6]. In addition to the abovementioned findings, the influence of polymer initial weight average molecular weight (M_{w0}) on the degradation rate cannot be disregarded. As a general rule, the higher the molecular weight is, the delayed degradation of the material is observed [22,23]. The other factor, controlling the degradation, refers to the glass transition temperature (T_g) and crystallinity of the material. However, it is considered to be a point of disagreement as diverse results are presented in the literature. A few of them state that faster degradation of the material is in general attributed to its lower molecular weight, as a reason of its low crystallinity [22], which agree with Alexis and co-workers study. They presented faster degradation of amorphous PDLLA than semi-crystalline PLLA.

Nevertheless, the size of investigated scaffold can also affect the degradation rate. According to Burkersoda and co-workers, the mechanism of erosion could be modified by changing i.e the dimension of the construct [24]. They pointed out that the size of polymer matrix larger than dimension of critical specimen lead to surface erosion. However, objects smaller than critical dimensions, experience bulk erosion. At the same time, it should be noted that critical dimensions differ significantly depending on the material type.

Besides the aforementioned examples, the internal architecture, which includes the selection of the lay-down pattern, pore size and porosity of the scaffolds, is of the importance from the TE point of view. Moreover, it can be easily modified, resulting in seeding efficiency [25–27] mechanical properties [8,28–30], [31] and finally, might influence the rate of hydrolytic degradation by changing the permeability of the scaffolds [32,33].

As the porosity of the scaffolds is generally known to control the degradation rate of 3D printed polymeric scaffolds, Hofmann and co-workers presented that lower porosity of the constructs contributed to the faster degradation, which could be explained by an autocatalysis effect of the acids in PLGA samples [34]. Wu and Ding observed similar effect in PLGA 85/15 scaffolds during 26 weeks of degradation conducted in PBS at 37 °C [35]. They investigated the relationship between the porosity of the scaffolds (80–95%) and pore size (50–450 μm) on the degradation kinetics. They explained that slow diffusion and high concertation of the degradation products in the case of smaller pore sizes is caused by larger wall thickness and accumulation of degradation products. On the other hand, Zhang et al. tested the effect of the porosity of PCL scaffolds during 72-weeks of degradation study. They verified that porosity could also induce faster degradation, especially when the porosity was more than 80% [36].

As the scaffold permeability could be one of the factors affecting the exchange of medium, Viana and coworkers investigated the influence of the pore architecture and pore size on the fluid flow by fabricating PCL scaffolds with the architecture of 0°/90°, 0°/60° and 0°/45° [32]. Overall, they indicated that constructs with 0°/90° lay-down pattern showed higher permeability and the most laminar fluid flow compared to the other ones. Moreover, they concluded that scaffolds permeability is more pore-size-dependent rather than influenced by filament lay-down pattern. Bartnikowski et al., on the other hand, introduced to 0°/90° and 0°/45° lay-down pattern an 0.5 inter-layer shift, which resulted in change of their permeability [26]. In order to exclude the effect of porosity, the scaffolds used in their study had a constant pore size. The computational fluid dynamic analysis revealed lower permeability in the scaffolds with filament offset.

Despite the given explanation about the effect of filament shift introduction on scaffolds permeability, as well as biological activity and mechanical properties in few references, to the best to our knowledge, none of the studies showed the effect of filament shift introduction on degradation of polymeric scaffolds.

Thus, in this study we aimed to investigate the relationship between the degradation rate and introduction of filament shift to the scaffolds fabricated by so called precision extruding deposition (PED). We decided to use two different copolymers, PLGA and PLCL and their TCP composites, containing 20 and 40 wt% of the filler. The constructs, with initial porosity ~60% were incubated in PBS up to 48 weeks. Change of initial molecular weight and mass loss were used as indicator of the degradation progress. Additionally, we investigated wettability of the bulk materials and permeability of the scaffolds.

2. Materials and methods

2.1. Materials

Copolymers of L-lactide and glycolide (PLGA) in an 82/18 M ratio and of L-lactide and ε-caprolactone (PLCL) in a 70/30 M ratio were purchased from Corbion Purac (The Netherlands). Tricalcium phosphate, TCP (particle size < 200 nm, puriss. P.a., ≥98% β-phase basis (sintered Powder)) and Phosphate Buffered Saline (PBS) was obtained from Sigma-Aldrich (USA). Methylene chloride was bought from POCH (Poland).

2.2. Preparation of the scaffolds

Materials with different TCP content (Table 1) used to fabricate scaffolds were prepared by solvent casting technique. Briefly, TCP particles were suspended in methylene chloride under magnetic stirring for 2 h, after which the obtained suspension was placed in an ultrasonic bath to ensure homogeneous dispersion of TCP particles. Subsequently, PLGA and PLCL copolymers were dissolved and stirred for 24 h. The as prepared slurry was cast into Petri dishes

Table 1
Composition of materials used for fabrication of the scaffolds by PED.

Material	PLGA (wt%)	PLCL (wt%)	TCP (wt%)
PLGA	100	-	-
PLGA/20TCP	80	-	20
PLCL	-	100	-
PLCL/20TCP	-	80	20
PLCL/40TCP	-	60	40

and dried in fume hood overnight and in a vacuum dryer at 45 °C and pressure of 50 mbar for 48 h.

The obtained bulk materials were cut and used to fabricate scaffolds by means of modified fused deposition modelling utilizing Bioscaffolder device (SYSENG, Germany), with the process parameters given in Table 2. The scaffolds were designed as cuboids with dimensions of 5.9 × 5.9 × 3.0 mm and 0°/90° lay-down pattern between fibres in neighbouring layers. Additionally, filament shift equal to half of the theoretical pore size (i.e. 0.325 mm) was introduced to n+2 layer (each second layer with the same fibre orientation), as shown in Fig. 1. The inner diameter of the nozzle used for extrusion of the filaments was equal 0.33 mm.

2.3. Scanning electron microscopy (SEM)

SEM was used to observe the cross-sections of fabricated scaffolds and capture changes occurring during degradation study. Phenom ProX microscope (Phenom World, The Netherlands) was used to investigate the morphology of dry specimens in a high resolution mode with acceleration voltage of 10 kV and secondary electron mode on. Scaffolds were not sputtered prior to SEM observations.

2.4. μCT

PLGA- and PLCL-based non-shifted and shifted scaffolds (3 scaffolds from each batch) were scanned using SKYSCAN 1174 (Bruker, Belgium). The study was conducted with the following parameters: X-ray tube voltage – 35 kV and current – 250 μA, performing 180-degree rotation with a step size of 0.8° and the voxel size was 10.08 × 10.08 × 10.08 μm^3. The obtained images were later reconstructed and analysed with the instrument software NRecon (SkyScan, Belgium) and CTAn (SkyScan, Belgium) in order to calculate the porosity of the scaffolds and their surface area-to-volume ratio (SVR). The reconstructed images were later visualized in 3D using Microsoft 3D Viewer software.

2.5. Thermogravimetric analysis (TGA)

In order to determine the mass percentage TCP particles dispersed in polymer matrices, thermogravimetric analysis of the composite films and non-degraded 3D printed samples was performed using thermogravimetric analyser Q5000 (TA Instruments, USA). Approximately 15 mg of the composite was heated at rate of 10 °C/min up to 600 °C under nitrogen atmosphere (flow of 25 ml/min). The residual mass was taken as an equivalent of the content of TCP nanoparticles present in the polymer matrix.

Q5000 thermogravimetric analyser was also used to determine the content of TCP in degraded samples. ~10 mg of each specimen was heated up to 700 °C, at heating rate of 50 °C/min with the nitrogen flow of 25 ml/min.

2.6. Post-treatment of PLCL-based scaffolds

Since crystallinity of PLCL-based scaffolds changed during storage from amorphous after printing to semi-crystalline after several weeks of storage, we decided to reduce its variability by annealing the PLCL-based samples at increased temperature. To that end, the scaffolds were incubated at 50 °C for up to four days.

Table 2
Printing parameters for different types of materials.

Parameter	PLGA-based samples	PLCL-based samples
inner diameter of the needle	330 μm	
temperature range	185–195 °C	160–175 °C
Pressure	4.5 bar	4.0–4.5 bar

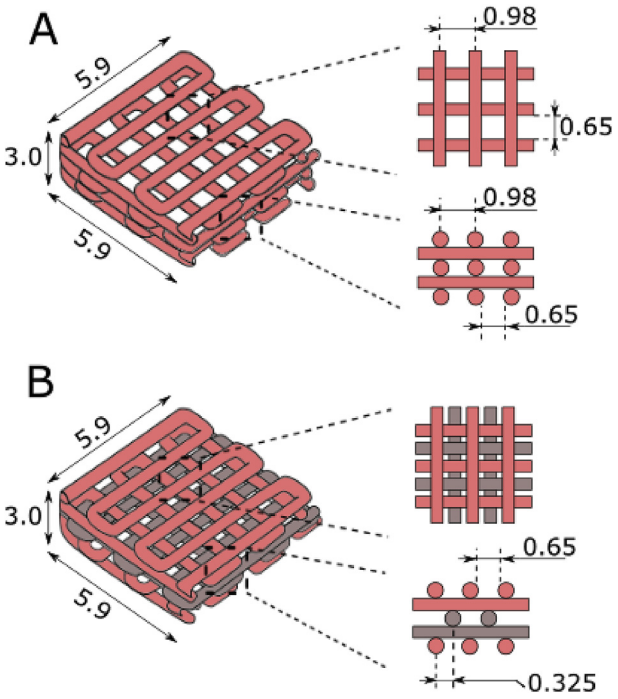

Fig. 1. Schematic arrangement of fibres in the architecture of exemplary scaffolds. Scaffolds with 0°/90° lay down pattern without filament shift (A) and scaffolds with filament shift in n+2 layer (grey-coloured) (B). All dimensions are given in mm.

2.7. Differential scanning calorimetry (DSC)

Change of crystallinity of PLCL-based samples during annealing were investigated using differential scanning calorimeter Q2000 (TA Instruments, USA) under nitrogen atmosphere (flow of 50 mL/min). Samples of ~8 mg were heated-cooled-heated from 0 °C to 150 °C, at heating and cooling rate of 10 °C/min.

2.8. Water contact angle

In order to determine surface wettability of the five tested materials, we conducted water angle measurements using sessile drop method by means of goniometer (Contact Angle System, OCA, Dataphysics), where the water drop size equalled 3 μL. The measurements of wettability were performed at room temperature on solvent casted films due to porous nature of the scaffolds.

2.9. In vitro degradation study in phosphate buffered saline (PBS)

The fabricated scaffolds were pre-wetted in PBS solution using centrifuge at 4022 g for 5 min. Three samples of each material and different architecture were immersed in 5 ml of PBS containing 0.02% sodium azide, with the initial pH of 7.4. The medium was changed every two weeks. The degradation study was carried out at 37 °C under agitation of 110 rpm for the period of 48 weeks. At subsequent time points, the samples were removed, rinsed with distilled water, weighted and left for drying in a fume hood overnight and later in a vacuum dryer (50 mbar, 25 °C) for about 7 days. In the meantime, pH of the medium was determined using the pH meter (Mettler Toledo, USA). The mass loss of the dry samples was calculated with equation (1):

$$\Delta m = \frac{m_0 - m_{dry}}{m_o} \; x\; 100\% \quad (1)$$

where m_0 is an initial dry weight of the sample, m_{dry} is the mass of the dry sample after degradation.

Water absorption (WA) was determined with equation (2):

$$WA = \frac{m_{wet} - m_{dry}}{m_{dry}} \; x\; 100\% \quad (2)$$

where m_{wet} is the mass of the wet sample, measured after removal from the medium, washed with distilled water and before leaving the specimen for drying.

2.10. Gel permeation chromatography (GPC)

The loss of the molecular weight of the samples was measured by means of GPC using refractive index detector (Agilent Singapore). Samples were dissolved in HPLC-grade chloroform (Chempur, Poland) at concentration of 2 mg/ml overnight. The TCP particles were removed by centrifugation at 9500*g* for 10 min. Aliquots of 100 μl of the polymer solution were injected into chloroform and separated on two linear coupled SEC columns (PLgel 5 mm MIXED-C, UK, 300 × 7.5 mm) at 35 °C and a flow rate of 0.7 mL/min. The system was calibrated using 9 polystyrene standards (Agilent, UK) with known molecular weights (Mp ranging from 580 g/mol to 990,500 g/mol).

2.11. Atomic force microscopy (AFM)

To observe changes in topography during in vitro degradation, topography visualization of the non-shifted and shifted scaffolds was performed using MFP 3D BIO (Asylum Research/Oxford Instruments). The microscope was operating in semi-contact regime (AFM S–C). Knowing that even slight changes in the ambient temperature (23 °C) and humidity (25%) affect the accuracy of the surface quality assessment, we ensured stable and controlled experiment conditions by enclosing the AFM in a chamber custom made to prevent temperature fluctuations. To register high-resolution topographical maps, silicon AC200TS (Olympus) scanning probes were used. According to the manufacturer, the probe is characterized with a spring constant of about ca. 9 N/m. The radius of the tip used for the imaging was estimated using calibration grating provided by the microscope manufacturer. Prior to the experiment, calibration grating was imaged in semi-contact mode and topographical imaging was used for the tip size estimation, which was done using integrated microscope software. IgorPro (ver. 6.17), a dedicated professional software provided by the microscope manufacturer was used for data analysis. Based on that protocol, the tip radius was determined to be 11 nm. Samples were imaged over an area of 5 × 5 μm and 2 × 2 μm at 0.6–1.0 Hz.

2.12. The fluid flow simulation

To explain the role of hydraulic permeability in hydrolytic degradation of porous scaffolds, the numerical simulation of fluid flow was carried out. The flow across non-shifted and shifted scaffolds was simulated using ANSYS Fluent software. The size of representative scaffold volumes was 4 mm × 4 mm × 3 mm [37]. The inlet velocity was equal to 0.0004 m/s, which guarantees laminar fluid flow. The Newtonian fluid flowing through the scaffolds was water. The permeability of porous scaffolds was calculated based on Darcy's Law (equation (3)), which relates the volumetric flow rate and induced pressure difference in a permeable matrix:

$$k = \frac{Q\mu L}{A\Delta P} \quad (3)$$

where k is the hydraulic permeability, Q - the fluid flow rate, L - the porous length, A - the cross section, ΔP - the pressure drop and μ the dynamic fluid viscosity.

2.13. Statistical analysis

Data are expressed as a mean ± standard deviation (SD). Two-way ANOVA followed by Tukey multiple comparison was performed using GraphPad Prism version 7.0 for Mac OS X, GraphPad Software, La Jolla California USA, where p value 0.0332 (*), 0.0021 (**), 0.0002 (***) and <0.0001 (****).

3. Results

3.1. Degradation of the scaffolds

The mass of fabricated scaffolds decreased with immersion time in PBS for all investigated scaffolds. As it can be seen in Fig. 2,

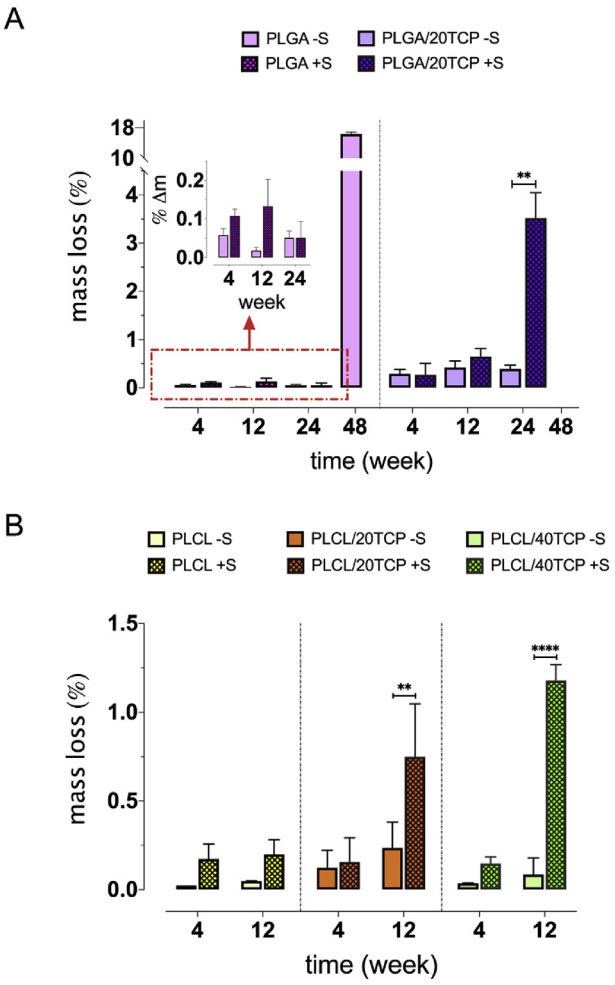

Fig. 2. Change of mass of PLGA- (A) and PLCL-based (B) scaffolds; non-shifted scaffolds (-S), shifted ones (+S); Disintegration of shifted PLGA, non-shifted and shifted PLGA/20TCP
samples was observed at week 48; p value 0.0332 (*), 0.0021 (**), 0.0002 (***) and <0.0001 (****).

materials with higher content of TCP had a higher mass loss comparing to the pristine polymeric scaffolds. The architecture had no significant effect on mass loss of pristine PLGA constructs during 24-weeks of immersion period. The degradation of PLGA scaffolds increased during following 24 weeks. However, the mass loss of shifted constructs could not be measured due to their disintegration. The non-shifted PLGA scaffolds were the only which sustained mechanical integrity over the entire period of the degradation, and their mass loss was 16.3 ± 0.6% at week 48. On the other hand, introduction of filament shift significantly increased the mass loss of the PLGA/20TCP scaffolds, which reached 3.5 ± 0.5% (vs. 0.4 ± 0.1% in the case of non-shifted ones) at week 24. The mass loss of shifted and non-shifted PLGA/20TCP scaffolds was not reported herein as their disintegration was observed.

Similar trend was observed for PLCL-based composite scaffolds (Fig. 2B) with the difference that the mass loss could not be measured after week 12 due to their disintegration. The highest weight loss (1.2 ± 0.1%) occurred for the samples with filament shift containing 40 wt% of TCP particles, contrary to the non-shifted scaffolds, which mass loss reached 0.1 ± 0.03%. In the case of shifted PLCL/20TCP scaffolds, significant decrease in mass was measured at week 12 for shifted and non-shifted constructs (0.8 ± 0.2% vs. 0.2 ± 0.05%, respectively). The similar trend was also noted for the scaffolds made of pristine PLCL, in which shifted constructs had higher mass loss comparing to the non-shifted ones.

Profile of pH for PLGA- and PLCL-based scaffolds is presented in Fig. 3. In case of PLGA and PLGA-20TCP scaffolds (A), similar tendency of pH decrement was measured up to week 30, when the drop in the pH of PLGA-based materials vary only from 7.4 to 7.3 maximally. After week 30, the decrease in pH up to week 48 was not observed only for non-shifted PLGA samples. The pH value decreased gradually for the rest of PLGA-based scaffolds, reaching its minimum equal ~6.1 at week 48. The course of pH changes for PLCL-based scaffolds was different, with the pH decreasing slightly starting from week 12 (disintegration of the samples proceeded) reaching its minimum equal ~6.6 at week 28. Henceforth, the pH started increasing and reached ~7.3 at week 48.

Fig. 4 depicts patterns of water absorption during the incubation period of 48 weeks. Introduction of filament shift had a significant effect on water absorption by pristine PLGA scaffolds at week 4 (18.9 ± 6.5%) and 12 (14.1 ± 3.7%), contrary to non-shifted constructs(4.4 ± 1.2% at week 4 and 4.3 ± 1.4% at week 12). However, it can be noticed that in the case of PLGA scaffolds containing 20 wt% TCP, introduction of filament shift led to significant water uptake increment at week 24, where the water absorption reached almost 80% of the initial value. This effect corresponds to the highest mass loss of the PLGA/20TCP specimens.

Profile of water absorption of PLCL-based scaffolds has a slightly different course comparing to the PLGA-based specimens. Water uptake for pristine PLCL samples during first 4 weeks of incubation period was similar for the shifted (9.4 ± 2.2%) and non-shifted(13.9 ± 3.1%) samples. The differences in water absorption at week 12 was 9.0 ± 2.1% and 4.5 ± 1.1% for shifted and non-shifted PLCL specimens, respectively. Profile of water absorption of PLCL/20TCP during degradation study was higher for constructs with filament shift, reaching 10.1 ± 3.4%, 18.8 ± 2.1% at week 4 and 12, respectively. Water uptake for shifted PLCL/40TCP scaffolds at week 4 (12.3 ± 4.5%) of degradation study was higher than in non-shifted constructs (4.7 ± 0.5%). However, this difference was not significant at week 4 and 12.

Table 3 depicts content of TCP in the samples used in the degradation study. As it can be seen, the content of bioactive ceramic in polymer matrix is consistent with the initial value at each fixed time point of degradation study. The TGA analysis of PLGA/20CTP constructs at week 48 and PLCL-based at week 24 and 48 were not presented in this study, as the disintegration of the samples was observed.

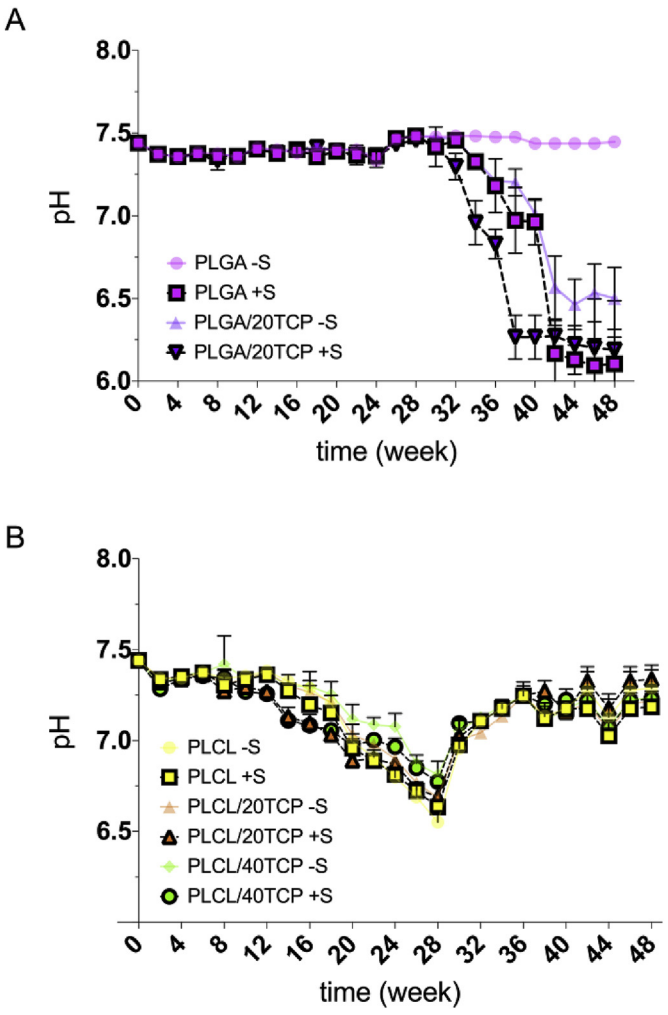

Fig. 3. Changes of pH of PBS during incubation periods for PLGA-based (A) and for PLCL-based scaffolds (B); non-shifted scaffolds (-S), shifted ones (+S).

3.2. Initial molecular weight loss

In Fig. 5, time evaluation of initial average molecular weight (M_{w0}) of the investigated scaffolds is shown at different time points of immersion in PBS. In general, PLCL and its composites degraded faster than pristine PLGA and PLGA/20TCP constructs (~90% decrease within 12 weeks for PLCL vs. 40% decrease within 24 weeks for pristine PLGA).

The decrease of initial molecular weight of PLCL-based constructs could be divided into two stages: the first – sharp and rapid, where the disintegration of samples was observed at week 12, and the second one, smoother (after week 12). The addition of TCP did not accelerate the degradation of PLCL-based constructs. There were also no significant differences in degradation profile of non-shifted PLCL-based scaffolds as well as in change of M_{w0} between PLCL/20TCP and PLCL/40TCP scaffolds within the same architecture groups. In PLCL and its composites, the decrease of M_{w0} was significantly different up to week 4 for pristine PLCL (~23% decrease within 4 weeks for non-shifted scaffolds vs. ~ 28% for shifted ones), PLCL/20TCP (~24% decrease within 4 weeks for non-shifted scaffolds

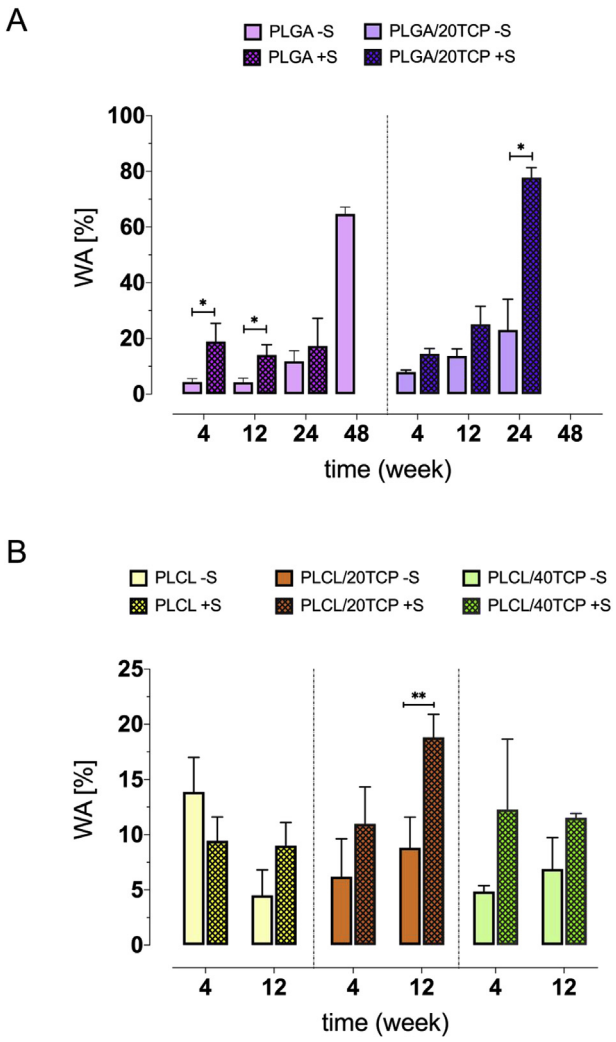

Fig. 4. Water absorption by PLGA-based (A) and PLCL-based constructs (B); non-shifted scaffolds (-S), shifted ones (+S); p value 0.0332 (*), 0.0021 (**), 0.0002 (***) and <0.0001 (****). The disintegration of shifted PLGA and non-shifted and shifted PLGA/20TCP
samples was observed at week 48.

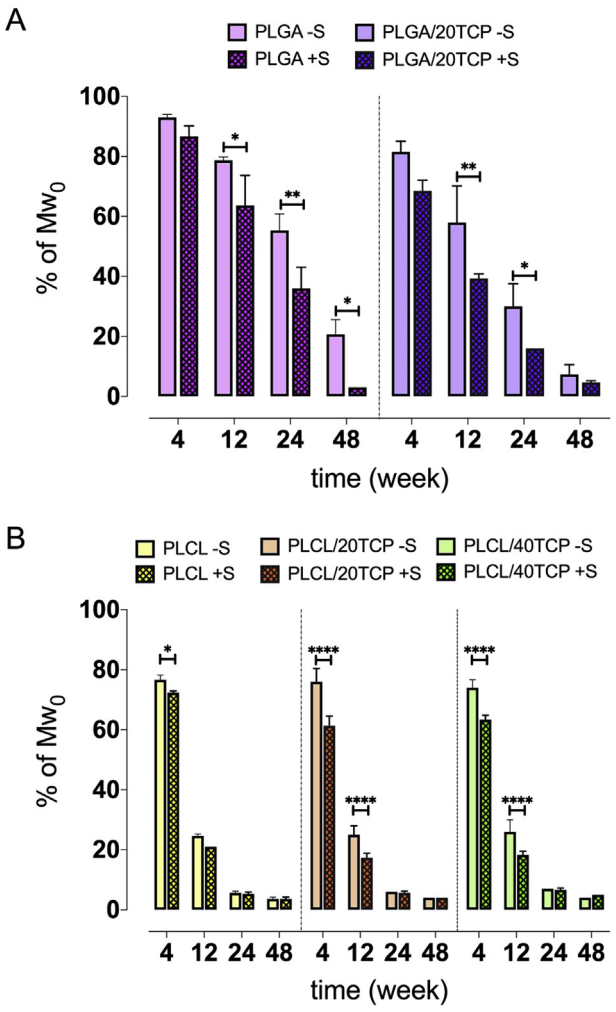

Fig. 5. Time evaluation of initial average molecular weight loss for PLGA-based (A), PLCL-based (B) scaffold; non-
shifted scaffolds (-S) and shifted ones (+S);
p value 0.0332 (*), 0.0021 (**), 0.0002 (***) and <0.0001 (****).

Table 3
Content of TCP in degraded composite scaffolds; results are given in percentage (%).

	PLGA/20TCP		PLCL/20TCP		PLCL/40TCP	
	no shift	shift	no shift	shift	no shift	shift
W0	21.1 ± 0.9		22.0 ± 0.8		41.1 ± 0.2	
W4	19.7 ± 0.3	19.8 ± 0.1	20.7 ± 0.5	20.7 ± 0.8	40.9 ± 0.5	40.1 ± 0.1
W12	19.4 ± 0.0	19.5 ± 0.1	20.3 ± 0.0	20.8 ± 0.1	40.8 ± 0.6	40.7 ± 0.1
W24	19.3 ± 0.2	19.1 ± 0.1	**disintegration of the samples**			

vs. ~ 39% for shifted ones) and for PLCL/40TCP (~26% decrease within 4 weeks for non-shifted scaffolds vs. ~ 37% for shifted ones).

In case of PLGA constructs, the introduction of TCP particles into polymer matrix hold more pronounced effect than in PLCL composites. As it is seen in Fig. 5B, the decrease of initial M_w of TCP-loaded PLGA scaffolds was higher than for pristine specimens up to week 48 of degradation (21.4% vs. 7% at week 4; 42% vs. 21.3% at week 12; 70% vs. 44.7% at week 24; 92.7% vs. 79.3% at week 48, for non-shifted TCP-loaded and TCP-free constructs, respectively). The addition of filament offset resulted in decrease of M_{w0} up to 70% within 24 weeks, and for PLGA/20TCP 80% decrease for shifted specimens vs. 70% decrease within 24 weeks for non-shifted ones. However, the significant differences in initial molecular weight of PLGA/20TCP constructs were observed up to week 12, which corresponds to disintegration of shifted PLGA/20TCP samples.

3.3. DSC measurements

DSC thermograms of PLCL/20TCP samples after printing and annealing at 50 °C up to 4 days (the results of crystallinity change and characteristic temperatures of PLCL and PLCL/40TCP are attached in supplementary data, Fig. A2) is presented in Fig. 6B. It was observed that samples after printing show amorphous character, contrary to PLGA-based specimens (Fig. 6A), as no melting peak occurred. Annealing the samples up to fourth day resulted in obtaining semi-crystalline structure. The decrease of glass transition temperature (T_g) of PLCL/20TCP constructs, as well as increase of melting enthalpy (ΔH_m), was observed within increasing time of annealing (Fig. 6B).

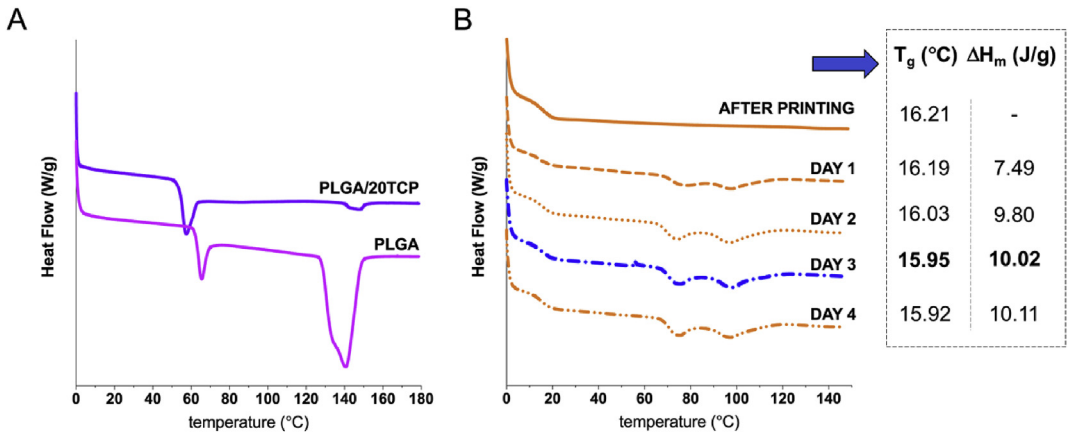

Fig. 6. DSC analysis of as-printed PLGA-based (A) and PLCL-20TCP samples (B) showing the change of crystallinity, glass transition temperature and melting enthalpy during annealing at 50 °C up to 4 days.

3.4. Surface morphology and internal morphology

3.4.1. SEM

Fig. 7 depicts changes in surface morphology of PLGA-based non-shifted and shifted scaffolds. The addition of TCP appeared to change surface morphology from smoother to rougher. The TCP particles also seemed to agglomerate in PLGA matrix, which can be seen in Fig. 7D. SEM images of degraded scaffolds were presented as a cross-sectional view of fibres at week 24, as no visible changes in surface morphology were observed at week 4 and 12. In case of non-shifted PLGA samples, the surface seemed to be smoother and the cracks, occurring at initial state, as the result of printing imperfections became less visible at week 24. Similar trend was detected in shifted PLGA scaffolds. However, it was amplified by additional small cavities in the material (red arrows in Fig. 7C). The most profound changes in surface morphology were noticed in PLGA/20TCP shifted constructs (Fig. 7F). The surface morphology of PLGA/20TCP samples with filament shift seemed to be rougher and filled with cavities, comparing to the initial state.

Fig. 8 shows SEM images of PLCL-based scaffolds at initial state

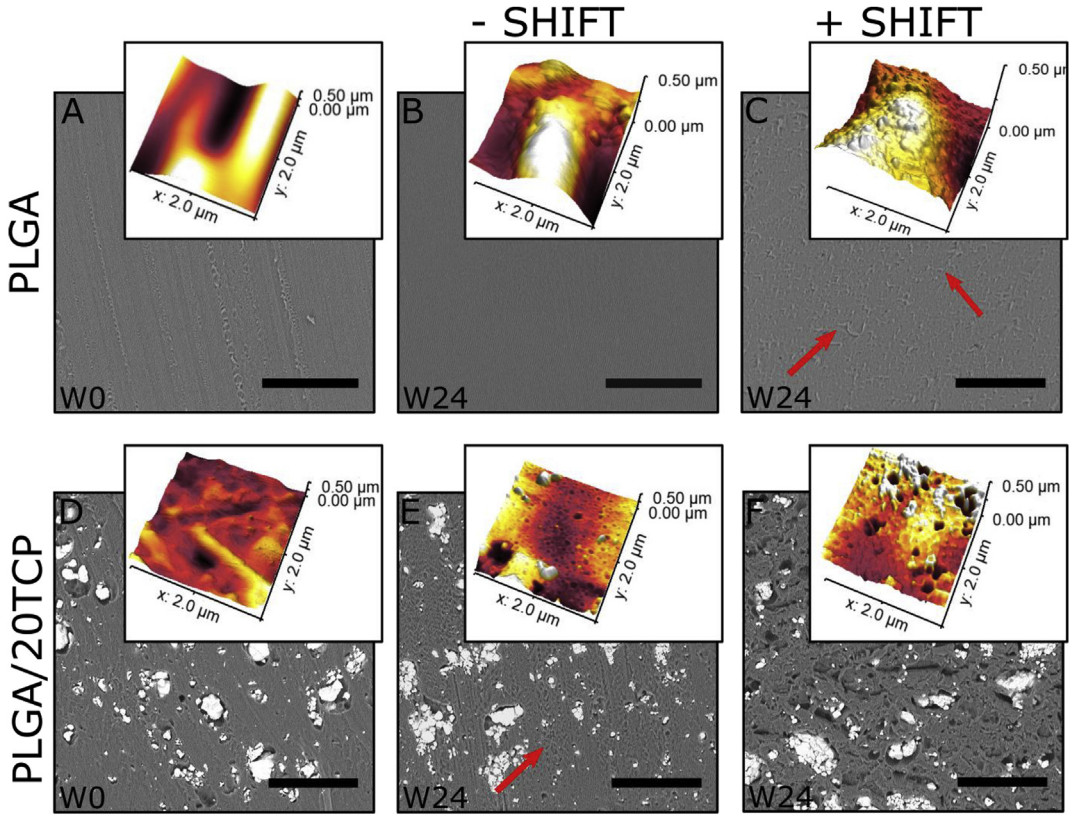

Fig. 7. Changes of surface morphology during degradation in PBS of non-shifted and shifted PLGA-based scaffolds. Figures represent cross-sectional view of the sample filaments. Scale bar 50 µm. The results from week 48 are not shown due to disintegration of the samples. Red arrows indicate small cavities in polymer matrix. Inset images show corresponding AFM topographical maps of the surface of investigated scaffolds. (For interpretation of the references to colour in this figure legend, the reader is referred to the Web version of this article.)

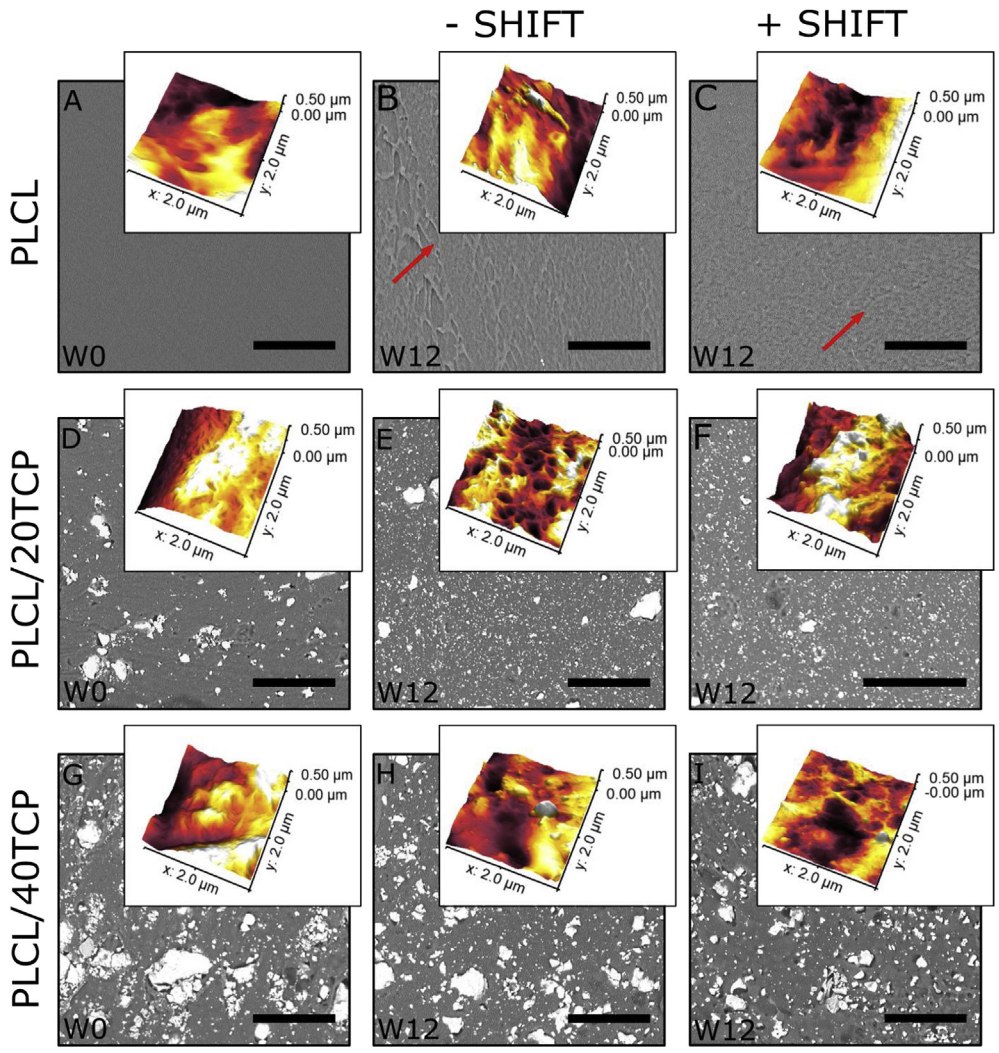

Fig. 8. Changes of surface morphology during degradation in PBS of non-shifted and shifted PLCL-based scaffolds. Figures represents cross-sectional surface of the filaments inside the scaffolds. Scale bar 50 µm. The results from week 24 and 48 are not shown due to disintegration of the samples. Red arrows indicate shrinking of the material. Inset images show corresponding AFM topographical maps of the surface of investigated scaffolds. (For interpretation of the references to colour in this figure legend, the reader is referred to the Web version of this article.)

and at week 12 of the degradation study, as the completely disintegration of the samples was observed henceforth. The surface of PLCL-based scaffolds become more wrinkled within 12 weeks of degradation study. In pristine PLCL constructs shrinking of the material might occurred, marked as red arrows on Fig. 8B and C. However, the significant differences between samples with and without filament shift could not be seen. Similar situation occurred in TCP-loaded PLCL composites, however the small pits at week 12 of degradation study were observed. In case of PLCL/40TCP specimens, the agglomeration of TCP particles at initial state could be also observed, comparing to samples made of PLCL/20TCP.

3.4.2. Topography visualization

AFM images (Figs. 7 and 8) revealed degradation-dependent alterations of scaffolds surface. Regardless of used polymer, pristine polymeric scaffolds (Figs. 7A and 8A) were characterized with rather smooth surface, which was evolving with time of degradation – especially for PLGA (Fig. 7A–C). In case of PLGA/20TCP scaffolds (Fig. 7E and F), cavities in the polymeric matrix were detected, and were more profound in case of shifted constructs. Regarding PLCL-based specimens at initial state (Fig. 8), ceramic particles were not visible on the surface (Fig. 8D and G). In general, degradation of composite PLGA and PLCL scaffolds could be divided into two stages, depending on architectural modifications. The first, where ceramics particles were visible on the surface of the scaffolds – especially in case of non-shifted ones. And the second one, where cavities in polymeric matrix were detected.

3.4.3. Microcomputed tomography

The visualization of region of interest of exemplary non-shifted and shifted PLGA/20TCP scaffolds is presented in Fig. 9. In both cases, scaffolds were designed and fabricated in 0°/90° lay-down pattern and with or without modifications of filament distance in n+2 layer, shifted (Fig. 9D–F) and non-shifted scaffolds (Fig. 9A–C) were obtained, respectively.

The µCT also allowed to determine the porosity and surface area-to-volume ratio (SVR) of non-shifted and shifted scaffolds, which are presented in Table 4. The porosity of shifted scaffolds was similar to those seen in non-shifted constructs. The porosity of pristine scaffolds was lower than TCP-loaded materials and was 57.3 ± 1.1%; 57.7 ± 3.4% and 52.0 ± 3.0%; 52.1 ± 3.0% for non-shifted and shifted PLGA scaffolds and non-shifted and shifted PLCL

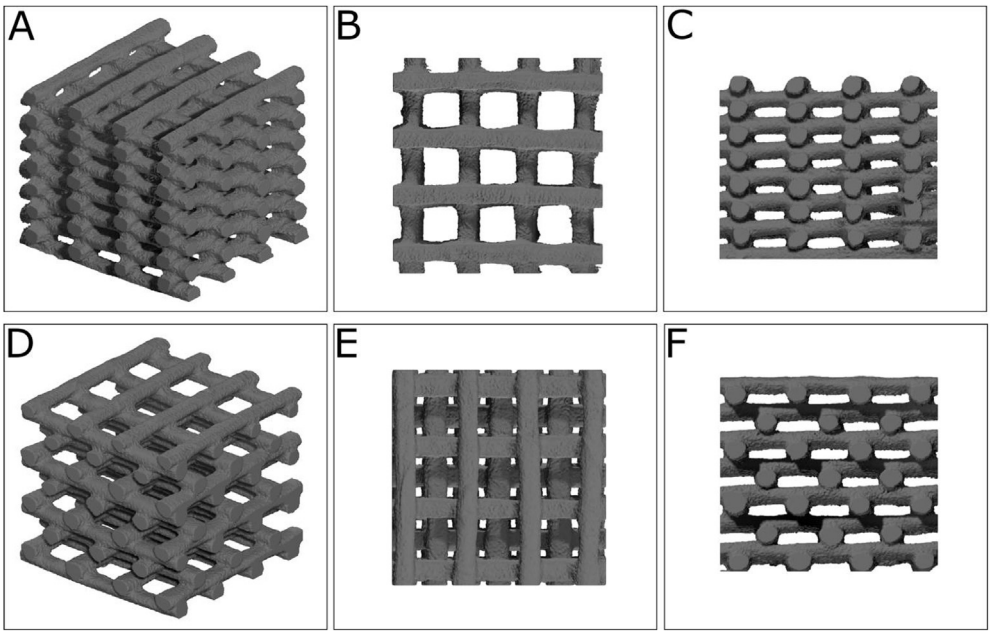

Fig. 9. The microcomputed visualization of the area of interest of exemplary non-shifted (A–C) and shifted PLGA/20TCP scaffolds (D–F).

Table 4
Porosity and Surface Area to Volume Ratio (SVR) of PLGA- and PLCL-based scaffolds determined by μCT.

Material	Porosity [%]		Surface Area/Volume Ratio (SVR) [mm^{-1}]	
	non-shifted	shifted	non-shifted	shifted
PLGA	57.3 ± 1.1	57.7 ± 3.4	12.7 ± 1.1	13.3 ± 1.2
PLGA/20TCP	60.3 ± 2.1	64.9 ± 3.4	13.8 ± 0.4	15.3 ± 1.0
PLCL	52.0 ± 3.0	52.1 ± 3.0	13.0 ± 0.8	12.3 ± 0.4
PLCL/20TCP	62.8 ± 0.9	66.6 ± 2.6	15.8 ± 1.3	17.5 ± 1.5
PLCL/40TCP	64.9 ± 1.8	62.3 ± 1.8	16.1 ± 1.0	18.9 ± 4.1

constructs, respectively. The lowest porosity, among all materials was observed in PLCL scaffolds. No significant differences were observed according to TWO-WAY ANOVA. The SVR, calculated by means of μCT software was greater in scaffolds with filament shift, except for pristine PLCL scaffolds. However, the statistical analysis did not show the significant differences between SVR of the two studied groups of architectures.

3.5. Wettability

As can be seen in Fig. 10, pristine PLCL and PLGA films showed the highest values of water contact angle, which equalled 105° ± 3° and 98° ± 5°, respectively. The addition of hydrophilic TCP decreased WCA to 84° ± 3°, 88° ± 3°, 84° ± 3° for PLGA/20CTP, PLCL/20TCP and PLCL/40TCP films, respectively.

3.6. Hydraulic permeability simulations

The simulations of fluid flow through investigated types of scaffold structures were carried out. The comparison of calculated hydraulic permeability of non-shifted and shifted constructs was presented in Fig. 11. The obtained results showed that the hydraulic permeability of non-shifted scaffolds is greater than permeability of scaffolds with filament shift, reaching 9.5e-9 and 7.75e-9 m^2, respectively. After characterizing the permeability of non-shifted and shifted scaffolds, Fig. 12 shows the fluid flow velocity

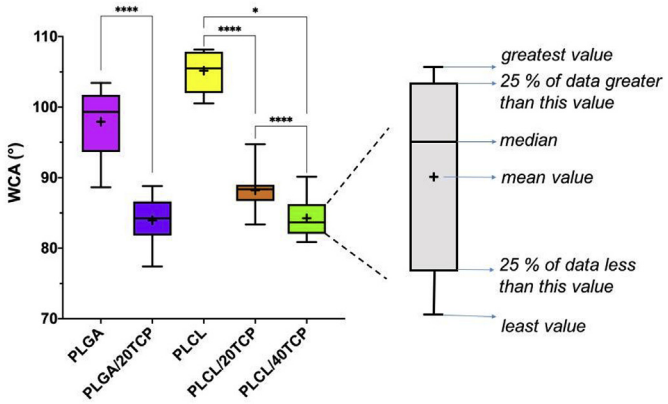

Fig. 10. Water contact angle of PLGA- and PLCL-based films calculated as a mean ("+" on the graph) of 10 measurements ± SD; p value 0.0332 (*), 0.0021 (**), 0.0002 (***) and <0.0001 (****).

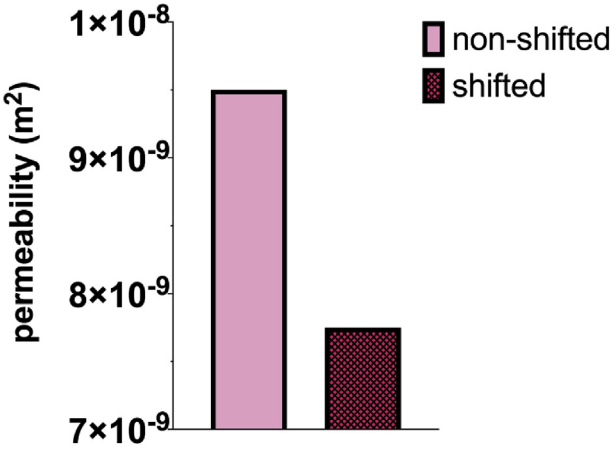

Fig. 11. Hydraulic permeability of shifted and non-shifted scaffolds.

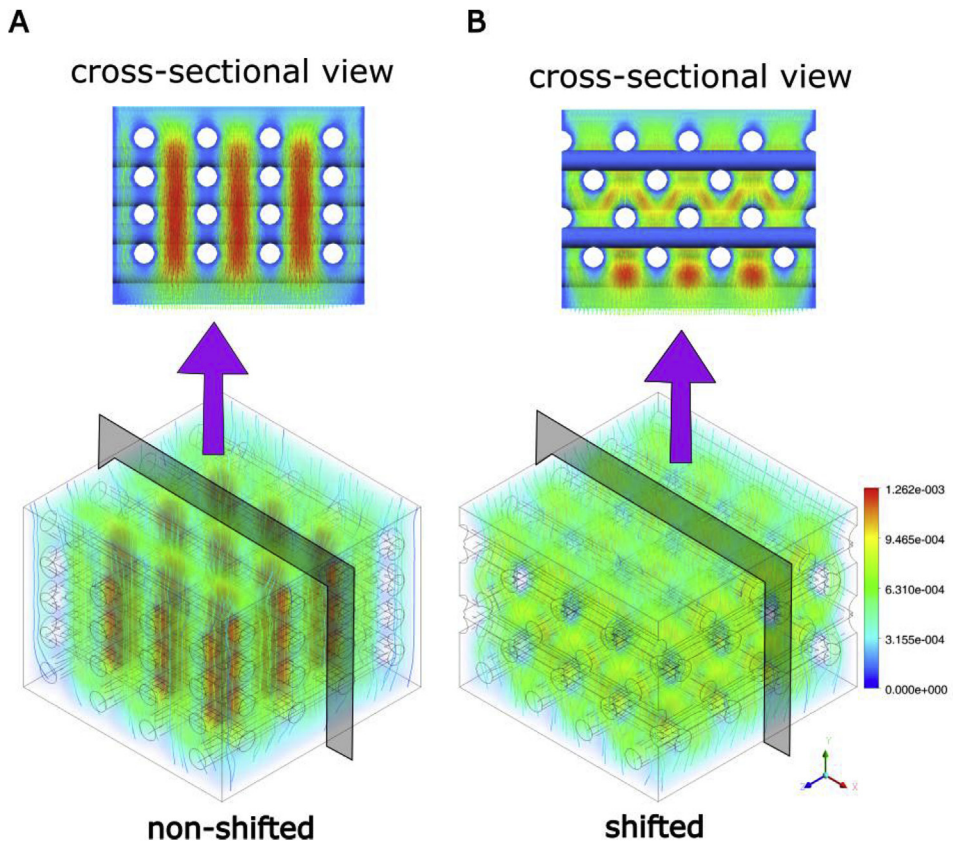

Fig. 12. Distribution of fluid velocity inside non-shifted (A) and shifted scaffolds (B) [m/s].

distribution inside two investigated groups of scaffolds. It is visible that the fluid flow distribution patterns varied with the architecture modifications. It is clearly noticeable that in case of shifted constructs, the flow is blocked by the scaffold's shifted filaments.

4. Discussion

In this study we aimed to investigate the effect of introduction of filament shift on degradation rate of scaffolds made of polymers and their composites. The scaffolds with two internal architectures, similar porosity and SVR were tested during in vitro degradation.

To describe the effect of filament shift introduction on degradation behaviour of scaffolds, there is a need to clarify the mechanism of polymers degradation. As it is well-known that biodegradable polyesters may undergo bulk and surface hydrolysis, depending on the size of the scaffold and reactivity of ester bonds, both of polyesters used in our study underwent bulk degradation and degraded prevailingly via chemical hydrolysis of ester bonds, causing the release of acids to the degradation medium [27,29,30]. Moreover, the structure of the constructs, namely their amorphous or semi-crystalline nature is one of the factors which may also affect the degradation kinetics [18]. As we observed that PLCL-based constructs are metastable and can change its nature due to physical aging and thus, affecting the degradation process, the fabricated scaffolds were annealed at 50 °C up to 4 days. In general, DSC thermograms revealed (Fig. 6) that only one day of annealing resulted in changing the amorphous nature of PLCL-based scaffolds to semi-crystalline (data for PLCL and PLCL/40TCP are attached in the supplementary data, Fig.A2). Similar phenomena was observed by Tsiuj and co-workers [41]. The authors observed changes in physical properties up to 180 days. The melting peak area after 3 days of storage in room temperature increased up to day 180. In our study PLCL-based constructs were annealed up to day three, as the differences in glass transition temperature and melting enthalpy between day three and four were not minor. Moreover, other study conducted by Fernandez revealed that PLCL copolymers with different LA:CL ratio showed similar physical changes in the structure as aforementioned [41]. They demonstrated that aging in PLCL is a physical process, in which primary chemical bonds are not involved with the undergoing changes in their structure. They also pointed that PLCL with the 70/30 content underwent dramatic changes in its behaviour during aging, changing the degree of crystallinity from amorphous up to crystallinity ranging 23% after 5 weeks of storage at 21 °C.

One of the main indicator in assessment of the degradation progress is the measurement of the scaffolds mass loss (Fig. 2). We observed no significant changes in mass loss of PLGA-based scaffolds during 24 weeks of degradation study. As we can see in Fig. 4, shifted PLGA/20TCP samples as the only showed the highest water uptake among all PLGA-based specimens. It may be assumed that addition of hydrophilic bioactive component, caused higher water uptake in places where no chemical bonds occurs. In this respect it is recalled that the introduction of the TCP can not only result in changing mechanical properties, cell performance in tissue engineering, but may also change the degradation kinetics by improving the wettability of the samples [6,25,42]. In our study, the decrement of water contact angle of pristine PLGA samples from 98° ± 5°—84° ± 3° for PLGA/20TCP (Fig. 10) was observed, making them hydrophilic and more exposed to absorb higher amount of PBS. Moreover, as hydrolysis of ester bonds proceeded, the molecular weight decreased, thus revealing more hydrophilic chain ends, which in fact can also absorb higher amount of water [18].

This finding is familiar with our study, in which % of M_{w0} of shifted PLGA/20TCP samples remained ~20% at the week 24 of degradation, in which water uptake was at the level of 80%. In addition, the introduction of filament offset resulted in accumulation of the degradation products, which in turn, caused faster mass loss and shrinking of the specimens. The effect of entrapment of degradation products in the tortuous architecture of shifted scaffolds also agreed with the weight loss of PLCL-based structures. The onset of significant pH decrease of PLCL-based specimens occurred after week 12 of degradation, which corresponds to disintegration of scaffolds (Fig. 2B) and decrease in initial molecular weight (Fig. 5B). We believe that the increase of pH, starting from week 28 in the case of PLCL-based scaffolds was caused by combination of two factors, namely, disintegration of scaffolds and exchange of the PBS [43–45]. In such instance, we assume that the mass loss of degraded samples was high enough that the number of acidic products of degradation diffusing to PBS was in fact low enough to play a significant role in lowering the pH of PBS. In addition, those water-soluble oligomers could be also removed during exchange of the PBS, which took place every second week [43]. The PLCL-based scaffolds underwent hydrolytic degradation faster than the PLGA-based ones, probably due to lower glass transition (T_g) point. Thus, the pH values for PLGA-based samples remained constant during 30 weeks of degradation study. As the experiment was conducted in PBS, which was exchanged in 2-week intervals, the buffer solution prevented pH from massive changes. The number of oligomers diffusing to PBS finally lead to decrease in pH, starting at week 30. However, the increase of pH, which was observed in case of PLCL-based constructs, could not be register for PLGA-based specimens as the degradation was conducted only up to week 48.

The mass loss of polymeric or composite scaffolds is preceded by hydrolytic degradation of polymer chains. Therefore, the measurement of molecular weight is an important indicator in monitoring the progress of biodegradation. As precision extruding deposition was adopted in case of fabrication of PLGA- and PLCL-based scaffolds, it was expected to obtain samples with the same parameters (i.e porosity, fibre diameter, weight average molecular weight) during the printing session. Notwithstanding this fact, the yellowing of the samples made of PLGA/20TCP was observed at the time of printing in high temperature (~185 °C) and decrement of initial Mw up to 50% was noted during 3 h of fabrication period (not presented in this study). According to Chia and co-worker work, polymers with high glass transition temperature (40–60 °C), such as PLGA, are not suitable for fused deposition modeling due to necessity of heating the material to high temperatures to provide them required flow during printing [46]. As it has been reported elsewhere, initial Mw could contribute to accelerated/delayed degradation of the material, specimens from different time points of printing and different sessions were selected to the degradation assay to unify the results [47,48]. The initial M_{w0} loss was presented as the ratio of Mw of the degraded part of the scaffold to the non-degraded slice, which was kept in the desiccator until the certain samples were removed from PBS at scheduled time point of degradation study.

What can be observed in Fig. 5A, the loss of M_{w0} proceeded gradually for PLGA-based specimens. However, the addition of hydrophilic TCP induced the degradation process for both shifted and non-shifted constructs. Reduction of initial Mw to the value below 20% resulted in disintegration of the samples. Shifted PLGA/20TCP constructs, among the PLGA-based specimens, as the first started to crumble at week 12 and the process of disintegration proceeded until week 48 (the rough structure seen in SEM images – Fig. 7C). Nevertheless, the TGA results revealed that there were no significant differences in TCP content in shifted and non-shifted scaffolds within 24 weeks of degradation. Therefore, it can be concluded that the polymeric matrix started to disintegrate, resulting in leaching of TCP particles. As SEM images did not give us a clear situation with the ongoing changes in surface morphology during degradation period, working principle of atomic force microscope (mechanical contact of sharp scanning tip probe with the surface of the sample) [49–51] enabled the inspection of 3D topography changes. The cavities in the surface of PLGA/20TCP scaffolds were observed, especially for shifted ones (Fig. 7F), which in fact corresponded to the size of ceramic particles (c.a 80–110 nm).What is interesting, non-shifted samples made of PLGA/20TCP degraded in similar way as shifted PLGA constructs, in which M_{w0} loss was observed at the similar level. This clearly shows that introduction of shift could accelerated degradation of PLGA matrix in a similar way as addition of 20 wt% of TCP particles. The effect of filament shift needs to be clarified herein. Since initial porosity of the scaffolds was similar for shifted and non-shifted specimens (significant differences were not observed according to two-way ANOVA), therefore it is unlikely that it could contribute to the faster initial molecular weight loss of shifted samples. The explanation of this dependency may lie behind a surface area concept, as it is believed that scaffolds with higher surface area or surface are to volume ratio will degrade faster due to higher accessibility of the polymer surface to water molecules [52]. To check if the introduction of filament shift to the group of scaffolds resulted in increment of surface area, the μCT was performed and with the use of instrument software, surface area to volume ratio for each architecture and each material was calculated (Table 4). No significant differences between non-shifted and shifted samples were observed. Thus, the theory of increment in surface area could not be used in explanation of faster degradation of shifted samples. An explanation about SVR given by Chew and co-workers could also help to understand the abovementioned findings [52]. They presented that SVR is not the only factor, which can play a crucial role in accelerating degradation, as it is commonly believed. In their study, the PLGA globular specimens with the lowest SVR experienced the fastest degradation. They concluded that not only SVR, but also porosity and entrapment of degradation products are involved in degradation kinetics. To check if the effect of filament shift will be also observed in different polyester-based constructs, PLCL-based scaffolds were also used in degradation experiment. The tendency of faster degradation in shifted PLCL-based scaffolds was in this case also observed. However, the differences in initial Mw decrease were not that clearly visible between shifted and non-shifted samples (Table 5). The disintegration of PLCL-based constructs proceeded at week 12. Moreover, the higher amount of TCP particles in PLCL matrix, 20 and 40 wt%, did not affect degradation kinetics, contrary to PLGA-based samples. The decrease of initial Mw proceeded in the same way in case of addition of 20 and 40 wt% TCP particles to the polymer matrix. This effect was quite surprising due to the fact that addition of bioactive content resulted in decrease of WCA from 105° ± 3° for pristine PLCL to 88° ± 3° and 84° ± 3° for PLCL/20TCP and PLCL/40TCP scaffolds, respectively.

Table 5
The initial molecular weight loss (%) for PLCL-based constructs. Bolded values and marked as "*" indicate significant differences in initial Mw loss of shifted and non-shifted PLCL-based samples.

	PLCL		PLCL/20TCP		PLCL/40TCP	
	no shift	shift	no shift	shift	no shift	shift
W0	0.0	0.0	0.0	0.0	0.0	0.0
W4	**23.3**	**27.7***	**24.0**	**38.7***	**25.5**	**36.7***
W12	75.3	79.0	**75.0**	**82.7***	**74.0**	**81.7***
W24	94.3	94.5	94.0	94.3	93.0	93.0
W48	100.0	100.0	96.0	96.0	96.0	95.0

One possible explanation of the obtained results for PLCL-based specimens might be the neutralization of acidic products of degradation by ceramic particles, as previously reported [53]. However, this finding still do not give a proper explanation in case of accelerated degradation in case of TCP-loaded PLGA specimens. The role of ceramic nanoparticles in case of degradation of polyester-based scaffolds received a great deal of concrete attention. Since we have met some disagreement opinions on the effect of ceramic particles of polyester scaffolds' degradation in the literature, and its role on delaying [54,55] and accelerating [56,57] its degradation rate, we believe that nanoparticles of TCP might act like a plasticizer in case of PLGA-based samples. We observed decrease of initial molecular weight of TCP-loaded PLGA samples and decrease of its T_g, which is typical in case of plasticizing effect [58,59]. We believe that plasticizing effect might be also attributed to differences referring to polymer initial state. As the degradation study was conducted at 37 °C, pristine PLGA samples were at glassy state (T_g ~ 57 °C), whereas PLCL in the rubbery state (T_g ~ 21 °C). Therefore, the motions of the chain segments for pristine PLGA were hindered due to their tight packaging. The addition of TCP resulted in increase of free volume and wide range of local motions become possible. In contrary to, the addition of nanoparticles to pristine PLCL samples, resulted in reducing the average free volume, thus reducing the space available for reorganization of polymer chains during degradation. This, in our opinion, hindered the chain mobility by its immobilization [60–62]. In the light of this, we believe that addition of nano-TCP in case of PLGA caused a repulsive reaction, thus the T_g shifted to lower temperatures and led to accelerated segmental relaxation process. The segmental relaxation is known for controlling the diffusion, viscosity and rotation of monomers in polymers. However, the mechanism of accelerating hydrolytic degradation by introduction of ceramic particles is still unknown. Thus, we assume that the plasticizing effect of TCP particles contributed to accelerated degradation of PLGA-based samples, contrary to PLCL-based ones. However, the accelerating or delaying effect of nano-TCP particles on degradation behavior require better explanation.

As it was mentioned before, Chew and co-workers pointed that retention of the degradation products in the architecture of the scaffolds play a crucial role in the degradation kinetics, we decided to follow this step and a give simulation-based explanation to accelerated degradation observed in shifted constructs [38]. As we designed and fabricated the tortuous architecture of the shifted scaffolds, we assumed that the accumulation and entrapment of the degradation products in pores can lead to faster degradation kinetics, which is on the other hand, related to the permeability of the scaffolds. In order to check the permeability of fabricated scaffolds, the simulations of fluid flow were carried out. According to the hydraulic permeability of each group of scaffold presented on Fig. 11, the permeability of non-shifted scaffolds was greater than permeability of shifted ones. As mentioned before, that monomers and other products of hydrolytic degradation of aliphatic polyesters are released into the degradation medium [63], the medium motion contributes then in efficient removal of the acidic degradation products from the vicinity of the polymer matrix. This effect could significantly decrease the rate of polymer degradation. We hypothesize that the removal of degradation products is strongly dependent on medium flow through porous structure. The achieved medium velocity distribution inside the porous structure subjected to degradation was related to the hydraulic permeability, such that the higher permeability, the lower degradation rate of porous scaffold. In such situation, higher degradation rate of shifted scaffolds, could be explained by their lower hydraulic permeability. The value of scaffold hydraulic permeability is caused mainly by the scaffold structure tortuosity and porosity. The porosity of both of considered groups of scaffolds were similar, however shifted scaffolds were much more tortuous than non-shifted ones. The abovementioned findings are consistent with other study, in which numerically obtained values of permeability were similar to ours. Dias and co-workers presented in his work that scaffolds with 46–74% porosity and 0.5–0.7 mm pore size contributed to obtaining permeability of the constructs in the range of 7.81–15.31e-09 m^2 [36].

In the light of presented results of the effect of filament shift introduction on scaffold degradation behaviour, we pointed out that modification of scaffold architecture in the form of filament shift in n+2 layer may affect degradation kinetics. We also believe that the effect described in this study could be also observed in case of other materials degrading with the same mechanism, as the one presented for PLGA- and PLCL-based scaffolds. Thus, the theory of entrapment of degradation products in the tortuous architecture of the TE scaffolds could be also use in case of accelerating degradation of commonly used, long-term degrading PCL.

5. Conclusion

In the present study we demonstrated that introduction of filament shift into the PLGA- and PLCL-based scaffolds accelerated the degradation process. By simply modification of the scaffold 0°/90° lay-down pattern, higher decrease of initial Mw in case of shifted constructs was observed during 48 weeks of degradation study. We proposed that addition of filament shift changed the structure tortuosity, and thus, its hydraulic permeability, making the architecture more tortuous, hindering medium exchange and causing a build-up of degradation products. Therefore, modifications of scaffold architecture in form of filament shift should be carefully considered during the design process in bone tissue engineering applications.

Declaration of competing interest

The authors declare that they have no known competing financial interests or personal relationships that could have appeared to influence the work reported in this paper.

Acknowledgments

This work was supported by the National Centre for Research and Development (Poland) in the frame of BonTuMod project (contract no. 2/POLTUR-1/2016). Authors would also wish to acknowledge Scientific and Technological Research Council of Turkey (TUBITAK) support through Project No: 215M621.

Appendix A. Supplementary data

Supplementary data to this article can be found online at https://doi.org/10.1016/j.polymdegradstab.2019.109030.

References

[1] S. Stratton, N.B. Shelke, K. Hoshino, S. Rudraiah, S.G. Kumbar, Bioactive polymeric scaffolds for tissue engineering, Bioact. Mater. 1 (2016) 93–108, https://doi.org/10.1016/j.bioactmat.2016.11.001.

[2] J. Idaszek, W. Święszkowski, K.J. Kurzydłowski, Change of mechanical properties of PCL-based ternary composites scaffolds fabricated by solid freeform fabrication technique during in vitro degradation, Compos. Theory Pract. 12 (2012) 228–231.

[3] B. Dhandayuthapani, Y. Yoshida, T. Maekawa, D.S. Kumar, Polymeric scaffolds in tissue engineering application: a review, Int. J. Polym. Sci. 2011 (2011), https://doi.org/10.1155/2011/290602.

[4] A. Chlanda, P. Oberbek, M. Heljak, E. Kijeńska-Gawrońska, T. Bolek, M. Gloc, Ł. John, M. Janeta, M.J. Woźniak, Fabrication, multi-scale characterization and in-vitro evaluation of porous hybrid bioactive glass polymer-coated scaffolds

for bone tissue engineering, Mater. Sci. Eng. C 94 (2019) 516–523, https://doi.org/10.1016/j.msec.2018.09.062.
[5] G.H. Yang, M. Kim, G. Kim, Additive-manufactured polycaprolactone scaffold consisting of innovatively designed microsized spiral struts for hard tissue regeneration, Biofabrication 9 (2017), https://doi.org/10.1088/1758-5090/9/1/015005.
[6] J. Idaszek, A. Bruinink, W. Święszkowski, Delayed degradation of poly(lactide-co-glycolide) accelerates hydrolysis of poly(ε-caprolactone) in ternary composite scaffolds, Polym. Degrad. Stab. 124 (2016) 119–127, https://doi.org/10.1016/j.polymdegradstab.2015.12.020.
[7] F. Melchels, M. Domingos, T. Klein, J. Malda, P.J. Bartolo, D. Hutmacher, Additive manufacturing of tissues and organs, Prog. Polym. Sci. 37 (2012) 1079–1104, https://doi.org/10.1016/j.progpolymsci.2011.11.007.
[8] I. Zein, D.W. Hutmacher, K.C. Tan, S.H. Teoh, Fused deposition modeling of novel scaffold architectures for tissue engineering applications, Biomaterials 23 (2002) 1169–1185, https://doi.org/10.1016/S0142-9612(01)00232-0.
[9] S. Jyoti Kalita, S. Bose, H.L. Hosick, A. Bandyopadhyay, Development of controlled porosity polymer-ceramic composite scaffolds via fused deposition modeling, Mater. Sci. Eng. C 23 (2003) 611–620, https://doi.org/10.1016/S0928-4931(03)00052-3.
[10] E. Ceretti, P. Ginestra, P.I. Neto, A. Fiorentino, J. Silva, Multi-layered scaffolds production via fused deposition modeling (FDM) using an open source 3D printer: process parameters optimization for dimensional accuracy and design reproducibility, Procedia CIRP 65 (2017) 13–18, https://doi.org/10.1016/j.procir.2017.04.042.
[11] K. Szlazak, J. Jaroszewicz, B. Ostrowska, T. Jaroszewicz, M. Nabiałek, M. Szota, W. Święszkowski, Characterization of three-dimensional printed composite scaffolds prepared with different fabrication methods, Arch. Metall. Mater. 61 (2016) 645–650, https://doi.org/10.1515/amm-2016-0110.
[12] L. Shor, S. Güçeri, R. Chang, J. Gordon, Q. Kang, L. Hartsock, Y. An, W. Sun, Precision extruding deposition (PED) fabrication of polycaprolactone (PCL) scaffolds for bone tissue engineering, Biofabrication 1 (2009), https://doi.org/10.1088/1758-5082/1/1/015003.
[13] F. Wang, L. Shor, A.L. Darling, S. Khalil, W. Sun, S. Güçeri, A.C.W. Lau, Precision extruding deposition and characterization of cellular poly-??-caprolactone tissue scaffolds, Rapid Prototyp. J. 10 (2004) 42–49, https://doi.org/10.1108/13552540410512525.
[14] C. Fedore, L.Y.L. Tse, H.K. Nam, K. Barton, N. Hatch, Analysis of polycaprolactone scaffolds fabricated via precision extrusion deposition for control of craniofacial tissue mineralization, Orthod. Craniofac. Res. 20 (2017) 12–17, https://doi.org/10.1111/ocr.12159.
[15] P.X. Ma, Scaffolds for tissue fabrication, Mater. Today 7 (2004) 30–40, https://doi.org/10.1016/S1369-7021(04)00233-0.
[16] J.C. Middleton, A.J. Tipton, Synthetic biodegradable polymers as orthopedic devices, Biomaterials 21 (2000) 2335–2346, https://doi.org/10.1016/S0142-9612(00)00101-0.
[17] S.H. Kim, Y. Jung, Resorbable polymers for medical applications, in: Biotextiles as Med. Implant, Elsevier, 2013, pp. 91–112, https://doi.org/10.1533/9780857095602.1.91.
[18] S. Lyu, D. Untereker, Degradability of polymers for implantable biomedical devices, Int. J. Mol. Sci. 10 (2009) 4033–4065, https://doi.org/10.3390/ijms10094033.
[19] L. Lu, C.A. Garcia, A.G. Mikos, In vitro degradation of thin poly(DL-lactic-co-glycolic acid) films, J. Biomed. Mater. Res. 46 (1999) 236–244, https://doi.org/10.1002/(SICI)1097-4636(199908)46:2<236::AID-JBM13>3.0.CO;2-F.
[20] L. Lu, S.J. Peter, M.D. Lyman, H.L. Lai, S.M. Leite, J.A. Tamada, S. Uyama, J.P. Vacanti, Robert Langer, A.G. Mikos, In vitro and in vivo degradation of porous poly(DL-lactic-co-glycolic acid) foams, Biomaterials 21 (2000) 1837–1845, https://doi.org/10.1016/S0142-9612(00)00047-8.
[21] T.G. Park, Degradation of poly(lactic-co-glycolic acid) microspheres: effect of copolymer composition, Biomaterials 16 (1995) 1123–1130, https://doi.org/10.1016/0142-9612(95)93575-X.
[22] F. Alexis, Factors affecting the degradation and drug-release mechanism of poly(lactic acid) and poly[(lactic acid)-co-(glycolic acid)], Polym. Int. 54 (2005) 36–46, https://doi.org/10.1002/pi.1697.
[23] D. Cam, S.H. Hyon, Y. Ikada, Degradation of high molecular weight poly(L-lactide) in alkaline medium, Biomaterials 16 (1995) 833–843.
[24] Friederike von Burkersroda, Luise Schedl, Achim Gopferich, Why degradable polymers undergo surface erosion or bulk erosion, Biomaterials 23 (2002) 4221–4231.
[25] M. Yeo, C.G. Simon, G. Kim, Effects of offset values of solid freeform fabricated PCL–β-TCP scaffolds on mechanical properties and cellular activities in bone tissue regeneration, J. Mater. Chem. 22 (2012), 21636, https://doi.org/10.1039/c2jm31165h.
[26] M. Bartnikowski, T.J. Klein, F.P.W. Melchels, M.A. Woodruff, Effects of scaffold architecture on mechanical characteristics and osteoblast response to static and perfusion bioreactor cultures, Biotechnol. Bioeng. 111 (2014) 1440–1451, https://doi.org/10.1002/bit.25200.
[27] B. Wysocki, J. Idaszek, J. Buhagiar, K. Szlązak, T. Brynk, K.J. Kurzydłowski, W. Święszkowski, The influence of chemical polishing of titanium scaffolds on their mechanical strength and in-vitro cell response, Mater. Sci. Eng. C 95 (2019) 428–439, https://doi.org/10.1016/j.msec.2018.04.019.
[28] D.W. Hutmacher, T. Schantz, I. Zein, K.W. Ng, S.H. Teoh, K.C. Tan, Mechanical Properties and Cell Cultural Response of Polycaprolactone Scaffolds Designed and Fabricated via Fused Deposition Modeling, 2001.
[29] L. Moroni, J.R. De Wijn, C.A. Van Blitterswijk, 3D fiber-deposited scaffolds for tissue engineering: influence of pores geometry and architecture on dynamic mechanical properties, Biomaterials 111 (2014) 1440–1451, https://doi.org/10.1002/bit.25200.
[30] J. Idaszek, E. Kijeńska, M. Łojkowski, W. Swieszkowski, How important are scaffolds and their surface properties in regenerative medicine, Appl. Surf. Sci. 388 (2016) 762–774, https://doi.org/10.1016/j.apsusc.2016.03.038.
[31] B. Wysocki, J. Idaszek, K. Szlazak, K. Strzelczyk, T. Brynk, K.J. Kurzydłowski, W. Świeszkowski, Post processing and biological evaluation of the titanium scaffolds for bone tissue engineering, Materials 9 (2016), https://doi.org/10.3390/ma9030197.
[32] T. Viana, S. Biscaia, H.A. Almeida, P.J. Bártolo, Permeability evaluation of lay-down patterns and pore size of PCL scaffolds, Procedia Eng. 59 (2013) 255–262, https://doi.org/10.1016/j.proeng.2013.05.119.
[33] C.G. Jeong, S.J. Hollister, Mechanical, permeability, and degradation properties of 3D designed poly(1,8 Octanediol-co-Citrate) scaffolds for soft tissue engineering, J. Biomed. Mater. Res. B Appl. Biomater. 93 (2010) 141–149, https://doi.org/10.1002/jbm.b.31568.
[34] D. Hofmann, M. Entrialgo-Castaño, K. Kratz, A. Lendlein, Knowledge-based approach towards hydrolytic degradation of polymer-based biomaterials, Adv. Mater. 21 (2009) 3237–3245, https://doi.org/10.1002/adma.200802213.
[35] L. Wu, J. Ding, Effects of porosity and pore size on in vitro degradation of three-dimensional porous poly(D,L-lactide-co-glycolide) scaffolds for tissue engineering, J. Biomed. Mater. Res. A 75 (2005) 767–777, https://doi.org/10.1002/jbm.a.30487.
[36] Q. Zhang, Y. Jiang, Y. Zhang, Z. Ye, W. Tan, M. Lang, Effect of porosity on long-term degradation of poly (ε-caprolactone) scaffolds and their cellular response, Polym. Degrad. Stab. 98 (2013) 209–218, https://doi.org/10.1016/j.polymdegradstab.2012.10.008.
[37] M.K. Heljak, K.J. Kurzydlowski, W. Swieszkowski, Computer aided design of architecture of degradable tissue engineering scaffolds, Comput. Methods Biomech. Biomed. Eng. 20 (2017) 1623–1632, https://doi.org/10.1080/10255842.2017.1399263.
[38] H. Zhang, L. Zhou, W. Zhang, Control of scaffold degradation in tissue engineering: a review, Tissue Eng. B Rev. 20 (2014) 492–502, https://doi.org/10.1089/ten.teb.2013.0452.
[41] H. Tsuji, A. Mizuno, Y. Ikada, Enhanced Crystallization of Poly (L -Lactide-Co- -Caprolactone) during Storage at Room Temperature, 1998, pp. 947–953.
[42] Z. Wang, Y. Wang, Y. Ito, P. Zhang, X. Chen, A comparative study on the in vivo degradation of poly(L-lactide) based composite implants for bone fracture fixation, Sci. Rep. 6 (2016) 1–12, https://doi.org/10.1038/srep20770.
[43] M. Elsawy, K.-H. Kim, J.-W. Park, A. Deep, Hydrolytic degradation of polylactic acid (PLA) and its composites, Renew. Sustain. Energy Rev. 79 (2017) 1346–1352, https://doi.org/10.1016/j.rser.2017.05.143.
[44] L.N. Woodard, M.A. Grunlan, Hydrolytic degradation and erosion of polyester biomaterials, ACS Macro Lett. 7 (2018) 976–982, https://doi.org/10.1021/acsmacrolett.8b00424.
[45] A. Gleadall, J. Pan, M.-A. Kruft, M. Kellomaki, Degradation mechanisms of bioresorbable polyesters. Part 1. Effects of random scission, end scission and autocatalysis, Acta Biomater. 10 (2014) 2223–2232, https://doi.org/10.1016/j.actbio.2013.12.039.
[46] H.N. Chia, B.M. Wu, Recent advances in 3D printing of biomaterials, J. Biol. Eng. 9 (2015) 1–14, https://doi.org/10.1186/s13036-015-0001-4.
[47] H.K. Makadia, S.J. Siegel, Poly lactic-co-glycolic acid (PLGA) as biodegradable controlled drug delivery carrier, Polymers 3 (2011) 1377–1397, https://doi.org/10.3390/polym3031377.
[48] A. Gleadall, J. Pan, M.A. Kruft, M. Kellomäki, Degradation mechanisms of bioresorbable polyesters. Part 2. Effects of initial molecular weight and residual monomer, Acta Biomater. 10 (2014) 2233–2240, https://doi.org/10.1016/j.actbio.2014.01.017.
[49] A. Chlanda, E. Kijeńska-Gawrońska, W. Święszkowski, E. Kijeńska, C. Rinoldi, M. Tarnowski, T. Wierzchoń, W. Swieszkowski, E. Kijeńska-Gawrońska, A. Chlanda, E. Choinska, N. Khenoussi, A. Tamayol, A. Khademhosseini, W. Święszkowski, Structure and physico-mechanical properties of low temperature plasma treated electrospun nanofibrous scaffolds examined with atomic force microscopy, Mater. Sci. Forum 6 (2018) 213–216, https://doi.org/10.1016/j.micron.2018.01.012.
[50] A. Chlanda, E. Kijeńska-Gawrońska, W. Święszkowski, Microscopic methods for characterization of selected surface properties of biodegradable, nanofibrous tissue engineering scaffolds, Mater. Sci. Forum 890 (2017) 213–216. https://doi.org/10.4028/www.scientific.net/MSF.890.213.
[51] C. Rinoldi, E. Kijeńska-Gawrońska, A. Chlanda, E. Choinska, N. Khenoussi, A. Tamayol, A. Khademhosseini, W. Święszkowski, Nanobead-on-string composites for tendon tissue engineering, J. Mater. Chem. B. 6 (2018), https://doi.org/10.1039/C8TB00246K.
[52] S.A. Chew, M.A. Arriaga, V.A. Hinojosa, Effects of surface area to volume ratio of PLGA scaffolds with different architectures on scaffold degradation characteristics and drug release kinetics, J. Biomed. Mater. Res. A 104 (2016) 1202–1211, https://doi.org/10.1002/jbm.a.35657.
[53] E. Díaz, I. Puerto, in vitro degradation of PLCL/nHA biodegradable scaffolds, Polym. Plast. Technol. Eng. 54 (2015) 556–564, https://doi.org/10.1080/03602559.2014.961087.
[54] L.M. Ehrenfried, M.H. Patel, R.E. Cameron, The effect of tri-calcium phosphate (TCP) addition on the degradation of polylactide-co-glycolide (PLGA), J. Mater. Sci. Mater. Med. 19 (2008) 459–466, https://doi.org/10.1007/s10856-006-

0061-6.
[55] D. Ege, S. Best, R. Cameron, The degradation behaviour of nanoscale HA/PLGA and α-TCP/PLGA composites, Bioinspired, Biomimetic Nanobiomaterials 3 (2014) 85–93, https://doi.org/10.1680/bbn.13.00027.
[56] C. Delabarde, C. Plummer, P.-E. Bourban, J.-A. Manson, Accelerated ageing and degradation in poly-L-lactide/hydroxyapatite nanocomposites, Polym. Degrad. Stab. 96 (2011) 595–607, https://doi.org/10.1016/j.polymdegradstab.2010.12.018.
[57] H. Li, J. Chang, pH-compensation effect of bioactive inorganic fillers on the degradation of PLGA, Compos. Sci. Technol. 65 (2005) 2226–2232, https://doi.org/10.1016/j.compscitech.2005.04.051.
[58] M.C. SHEN, A. V TOBOLSKY, Glass transition temperature of polymers, in: Plasticization Plast. Process, AMERICAN CHEMICAL SOCIETY, 1965, pp. 2–27, https://doi.org/10.1021/ba-1965-0048.ch002.
[59] P. Mencik, R. Prikryl, I. Stehnova, V. Melcova, S. Kontarova, S. Figalla, P. Alexy, J. Bockaj, Effect of Selected Commercial Plasticizers on Mechanical, Thermal, and Morphological Properties of Poly(3-hydroxybutyrate)/Poly(lactic acid)/Plasticizer Biodegradable Blends for Three-Dimensional (3D) Print, Mater, 2018, p. 11, https://doi.org/10.3390/ma11101893 (Basel, Switzerland).
[60] N. Wang, X. Wu, C.S. Liu, Opposite effects of SiO2 nanoparticles on the local alpha and larger-scale alpha' segmental relaxation dynamics of PMMA nanocomposites, Polymers 11 (2019), https://doi.org/10.3390/polym11060979.
[61] M. Roussenova, D.J. Hughes, J. Enrione, P. Díaz Calderón, E. Sivaniah, Q. Song, J. Ubbink, P. Beavis, A. Swain, M.A. Alam, Free volume, molecular mobility and polymer structure: towards the rational design of multi-functional materials, Acta Phys. Pol. Ser. A 125 (2014) 801–805, https://doi.org/10.12693/APhysPolA.125.801.
[62] T. Shmool, J. Zeitler, Insights into the Structural Dynamics of PLGA at Terahertz Frequencies, 2018, https://doi.org/10.26434/chemrxiv.6450545.v1.
[63] M.K. Heljak, W. Swieszkowski, K.J. Kurzydlowski, Modeling of the degradation kinetics of biodegradable scaffolds: the effects of the environmental conditions, J. Appl. Polym. Sci. 131 (2014) 1–7, https://doi.org/10.1002/app.40280.